Comparative study on the speckle filters for the very high-resolution polarimetric synthetic aperture radar imagery

Sheng Sun
Renfeng Liu
Changcai Yang
Huabing Zhou
Ji Zhao
Jiayi Ma

Comparative study on the speckle filters for the very high-resolution polarimetric synthetic aperture radar imagery

Sheng Sun,[a,]* Renfeng Liu,[b] Changcai Yang,[c] Huabing Zhou,[d] Ji Zhao,[e] and Jiayi Ma[f]

[a]Guangdong University of Technology, School of Computer Science, No. 1 Engineering Building, No. 100 Waihuan Xi Road, Guangzhou Higher Education Mega Center, Panyu District, Guangzhou 510006, Guangdong, China
[b]Wuhan Polytechnic University, 68 Xuefu South Road, Changqing Garden, Wuhan 430023, Hubei, China
[c]Fujian Agriculture and Forestry University, No. 15 Shangxiadian Road, Cangshan District, Fuzhou 350002, Fujian, China
[d]Wuhan Institute of Technology, 693 Xiongchu Avenue, Wuhan 430073, Hubei, China
[e]SAIT China Lab, 18F Taiyanggong Building, 12A Taiyanggong Mid Road, Chaoyang District 100028, Beijing, China
[f]Wuhan University, No. 299 Bayi Road, Wuchang District, Wuhan 430072, Hubei, China

Abstract. With the emergence of very high-resolution airborne synthetic aperture radar systems, it is necessary to reinvestigate these proposed methods with respect to their despeckling performances. As for the very high resolution polarimetric synthetic aperture radar (PolSAR) data, the presumption that the resolution cell is much larger than the radar wavelength becomes ineffective. Therefore, some classic and new filters are thoroughly reviewed. For the evaluation of speckle filters, both indicators for polarimetric information and spatial information are listed. The absolute relative bias is introduced, with the purpose of measuring the filtering performance concerning the indicators for polarimetric information. Moreover, the ratio of half power point width is employed to quantitatively assess the degree of point target preservation. A series of experiments are carried out based on the real PolSAR imagery which is obtained from an uninhabited aerial vehicle synthetic aperture radar system. It can be concluded that existing filters can only attain good performance with reference to part of the indicators. As regards very high-resolution PolSAR imagery, it is necessary to conceive more apposite new filters or make improved versions of the existing filters. © *The Authors. Published by SPIE under a Creative Commons Attribution 3.0 Unported License. Distribution or reproduction of this work in whole or in part requires full attribution of the original publication, including its DOI.* [DOI: 10.1117/1.JRS.10.045014]

1 Introduction

With newly released diversiform missions being finished, the spaceborne and airborne platforms of synthetic aperture radar (SAR) are booming. As is known to all, speckle filtering is one of the classic topics in the radar remote sensing community. However, it is observed that in-depth comparative studies on polarimetric synthetic aperture radar (PolSAR) data are few in number.[1] Especially, studies on data of the emerging airborne SAR systems, such as F-SAR,[2] uninhabited aerial vehicle synthetic aperture radar (UAVSAR),[3] and Pi-SAR2[4] that generally have large dimensions and very high resolution data in single, dual, and quad polarization configurations

---

*Address all correspondence to: Sheng Sun, E-mail: mycalos@gmail.com

are even fewer in number. The spatial resolution of these systems is often on a decimeter level and the dimensions are on the order of 10 to 20,000 by 10 to 20,000 pixels.[5] Therefore, it is necessary to begin an investigation into the filtering performance of speckle filters on very high-resolution PolSAR data.

A boxcar filter is the most fundamental and simplest means of speckle denoising. As with other PolSAR speckle filters, it uses a coherence matrix or covariance matrix as the processing objects. The underlying implementation strategy of a boxcar filter is to average all the matrix elements within a square window arithmetically. This simple procedure can maintain the polarimetric properties of certain pixels very well. However, it blurs the point targets, causes a mixture of heterogeneous pixels, and degrades the spatial details.[1] A series of filters developed by Lee et al., which are still blossoming, fill in part of these gaps. Scattering model-based speckle filter (SMB) was launched by Lee et al.[6] SMB first of all applies Freeman and Durden decomposition to the input PolSAR covariance matrix data, and divides all the pixels into three dominant scattering categories: surface, volume, and double-bounce scattering, which serve as the initial input data. Then all the pixels will be reclassified based on the Wishart distance model, which partially characterizes the statistical property of each pixel. Finally, the filtering kernel that minimizes the mean square error is applied, which is often found in the classic filters developed by Lee et al. for single polarization SAR data. The Lee et al. improved sigma filter (LeeSig) is a revised version of the classic one that was set forward for the single polarization SAR data.[7] To preserve the strong point targets, a calculation of 98% was conceived by Lee et al. The calculation acts as a preprocessing step that aims at distinguishing strong point targets from the other pixels. This filter fixes the deficiencies of the sigma range in the classic version. When implementing denoising, it adopts the minimum-mean-square-error kernel. Meanwhile, many significantly related explorations and experiments were done by Lopez-Martinez et al., who stated that the characterization of the multidimensional or multichannel speckle noise component played a pivotal role in the processing of PolSAR data.[8–11] They established a compound model that consists of a multidimensional, zero-mean, complex Gaussian random variable, and a random texture variable was established. They presented a model-based filter (MB) that processes the diagonal elements and off-diagonal elements differently.

As the core of an An-Yang filter, the pretest approach was devised by Chen et al.[12] It employs nonlocal noise filtering in optical image processing. It uses the similarity of patches rather than pixels to distinguish homogeneous pixels from heterogeneous pixels. The similarity between two patches is obtained and then converted into the weight that will be assigned to the corresponding homogeneous pixel. Finally, with corresponding weight for the homogeneous pixels, a boxcar-style average is carried out. Nonlocal means filter (NM), which also adopts the principle of nonlocal noise filtering, was introduced by Zhong et al.[13] It combines the structure similarity introduced by the NM filter with the homogeneity similarity introduced by the LeeSig filter. It behaves like the LeeSig filter when estimating the filtered covariance matrices. There is a significant difference between the An-Yang filter and NM, although they both originate from the nonlocal method. Mean shift-based algorithm (MS) was proposed by Lang et al.[14] The MS is well known and has been widely used in digital image filtering. Lang et al. proposed an adaptive variable asymmetric bandwidth selection approach as a major improvement of the conventional MS algorithm. It was reported by them that the newly derived generalized MS filter was applicable to both single polarization SAR and fully polarimetric SAR data. Following the speckle filtering principles for PolSAR data, a method that employs a nonlinear partial differential equation diffusion was proposed by Sun et al.[15] Nonlinear anisotropic diffusion is more flexible when filtering toward the orientation of interesting features. It suggests a scheme using edge-enhancing anisotropic diffusion and extends the conventional model to PolSAR speckle filtering.

The topic of speckle filtering is a core concern in the community of radar remote sensing and will always be noteworthy. Due to limited space, it is impossible to encompass all the newly proposed methods here. Validation and measurement for the rest of the filters deserve further investigation in the future. The rest of this paper is organized as follows. In Sec. 2, SAR polarimetry is briefly introduced. An exchange of views with respect to speckle-filtering principles is presented in Sec. 3. Both the qualitative and quantitative evaluations on very high-resolution PolSAR data are elaborated in Sec. 4. Finally brief conclusions are drawn in Sec. 5.

2 Basics of Synthetic Aperture Radar Polarimetry

In general, the incident and scattered waves by imaging radar are denoted by $\underline{E}_I$ and $\underline{E}_s$, respectively. With regard to the scattering process occurring at the target of interest, a matrix, called a scattering matrix, is commonly employed to express the relationship of the two waves. All the elements of the scattering matrix are called complex scattering coefficients. The diagonal elements of this matrix are commonly known as copolar terms and the off-diagonal elements are often called crosspolar terms. The former associates the incident waves with scattered waves when their polarization states are identical. The latter associates the incident waves with scattered waves when their polarization states are orthogonal.[16] This procedure is formalized in Eq. (1). λ is the radar wavelength and r is the distance from the observation point to the scatterer. The term $\frac{e^{\frac{2\pi jr}{\lambda}}}{r}$ takes into account the propagation effects both in amplitude and phase.

$$\underline{E}_s = \frac{e^{\frac{2\pi jr}{\lambda}}}{r} \begin{bmatrix} S_{11} & S_{12} \\ S_{21} & S_{22} \end{bmatrix} \underline{E}_I. \tag{1}$$

Furthermore, it is necessary to assign a specific coordinate system since the values of scattering matrix elements depend on the chosen coordinate system and polarization basis. In general, the horizontal-vertical basis is the most widely used for describing the coordinate system. The scattering matrix can be denoted as Eq. (2) in such a basis.

$$S = \begin{bmatrix} S_{11} & S_{12} \\ S_{21} & S_{22} \end{bmatrix} = \begin{bmatrix} S_{HH} & S_{HV} \\ S_{VH} & S_{VV} \end{bmatrix}. \tag{2}$$

The term S_{HH} corresponds to the power return when both the incident and scattered waves are in a horizontal polarization state. The denotation is similar for the remaining three items. According to the reciprocity theorem, the scattering matrix is symmetrical, $S_{HV} = S_{VH}$. For convenience of calculation, the scattering matrix is often expressed as a vector that is symbolized as Ω. This vector, listed in Eq. (3), is commonly called a target vector.

$$\Omega = \begin{bmatrix} S_{HH} \\ \sqrt{2}S_{HV} \\ S_{VV} \end{bmatrix}. \tag{3}$$

It is worth noting that not all the targets in a natural scene can be simply characterized by a scattering matrix. As a matter of fact, not all radar targets are stationary or fixed. Most natural targets change over time and consequently their scattered waves are no longer in a coherent, monochromatic, and completely polarized shape. In such cases, a new matrix, called a covariance matrix, is introduced to denote the scattering process of such targets that are called distributed targets. This matrix C_3, demonstrated in Eq. (4), employs the operator of ensemble average to characterize the distributed targets.[16] The superscript $*T$ denotes an operator of conjugate transpose.

$$C_3 = \langle \Omega\Omega^{*T} \rangle = \left\langle \begin{bmatrix} C_{11} & C_{12} & C_{13} \\ C_{12}^* & C_{22} & C_{23} \\ C_{13}^* & C_{23}^* & C_{33} \end{bmatrix} \right\rangle = \left\langle \begin{bmatrix} |S_{HH}|^2 & \sqrt{2}S_{HH}S_{HV}^* & S_{HH}S_{VV}^* \\ \sqrt{2}S_{HV}S_{VV}^* & 2|S_{HV}|^2 & \sqrt{2}S_{HV}S_{VV}^* \\ S_{VV}S_{HH}^* & \sqrt{2}S_{VV}S_{HV}^* & |S_{VV}|^2 \end{bmatrix} \right\rangle. \tag{4}$$

3 Discussion on the Polarimetric Synthetic Aperture Radar Speckle Filtering Principles

The principles that should be followed when designing a filter for alleviating the effect of PolSAR speckle are always a hotspot of research in this field. In previous studies, researchers, such as Lee et al.[5] and Lopez-Martinez et al.,[10] came up with different opinions from different

perspectives. As there is no universal agreement regarding these principles, it is a must to review related previous studies systematically. Lee et al. summarized the speckle filtering principles that are listed as follows: (a) for preserving the statistical characteristics, each term of the covariance matrix should be filtered in a manner similar to multilook processing by averaging the covariance matrices of neighboring pixels. (b) To avoid introducing crosstalk between polarization channels, it was required that each element of the covariance matrix should be filtered statistically independently of other terms. (c) To preserve polarimetric properties, only neighboring pixels with a similar scattering mechanism should be included in the filtering.[5,7] Lopez-Martinez et al.[10,11] stated that the above principles were established partly on the assumption of a multiplicative speckle noise model. In their opinion, the multiplicative speckle noise model might have to be extended in order to get a better characterization of speckle for the off-diagonal elements of the covariance matrix and Lee's principles might have to be relaxed. They continued to expound their views on the principles in Ref. 1 and emphasized that the first priority was to preserve the inherent scattering property of SAR data. It was illustrated that if each element of the covariance matrix was filtered separately then the correlation between polarizations would be affected. Lopez-Martinez et al. stated that diagonal terms and off-diagonal terms of a single covariance matrix were filtered entirely differently in Refs. 10 and 11. It was thus concluded that the correlation coefficients were no longer preserved.

Researches on filtering principles have remained compelling, e.g., in Ref. 1. It is well known that the object to be modeled and filtered is the second-order moments of the multidimensional SAR data, which is in the form of the covariance matrix or coherency matrix. It was assumed that these matrices contained all the necessary information to characterize the multidimensional SAR data. Nevertheless, Samuel Foucher et al. thought that this assumption was only valid for those pixels in stationary area. They also suggested that more evolved stochastic data models should be associated with the need to estimate additional stochastic moments.[1]

After review, two conclusions can be made. On the one hand, an agreement on adaptation to signal morphology is reached. This adaptation contains two aspects. It is required to maintain the spatial resolution and the radiometric amplitude in the case of point scatterers for one thing. For another, it is required, in the case of distributed scatterers, to perform an estimation of stationary pixels to build the covariance matrix. An indiscriminate average will cause a mixture of pixels that have different stationarity. At present, only the diagonal elements of the covariance matrix that contain the radiometric information are employed to identify the signal stationarity. Nevertheless, it has been pointed out that this may not be an optimal manner to estimate the pixel stationarity.[1,17,18] This topic deserves further study in the future.

On the other hand, the difference between the aforesaid two versions of despeckling principles lies in the processing of off-diagonal elements of the covariance matrix. The approach proposed by Ref. 5 suggested that all the elements of the covariance matrix must be filtered by the same amount. There is a basic fact that can be unfolded as follows. First, it is evident that the second-order moments, which are Hermitian matrices, are all positive semidefinite according to their constitution. For the subsequent polarimetric decomposition and classification, it is required that the filtered matrices remain to be positive semidefinite. After performing the filtering procedure, as follows from the principles in Ref. 5, the filtered matrices continue to be positive semidefinite. Second, it was reported that an extension to the principles in Ref. 5 had been made, which consisted of a more accurate PolSAR speckle noise model for the off-diagonal elements of the covariance matrix.[1] However, whether this revision can maintain the positive semidefiniteness remains to be seen.

4 Evaluation on Polarimetric Synthetic Aperture Radar Speckle Filters

It has been extensively recognized that the procedure of evaluation on speckle filters should be executed from two perspectives: (1) the analysis of the retrieval of the polarimetric information. (2) The assessment of the maintenance of spatial resolution and spatial details. The primary focus of this study is the despeckling performance evaluation on the airborne PolSAR imagery with very high resolution. For these very high resolution PolSAR data, the size of the resolution cell is close to that of the radar wavelength. One presumption for the fully developed speckle is that the

resolution cell is much larger than the radar wavelength. This assumption will be invalid in the case of very high resolution data, because the diameter of the resolution cell is only about 6 to 10 times larger than that of the radar wavelength.[19] A homogeneous area was used as an exemplification and the histograms for three diagonal elements of the covariance matrix were computed in Ref. [19]. It can be observed from the results that the values of three diagonal elements follow Gamma distributions.[19] In addition, it is found that the PolSAR image looks like an optical image when the size of the resolution cell is reduced to the extent that the speckle granularity is significantly smaller than the size of objects of interest. Speckle filtering, in Ref. [19], is deemed to be less important for some applications based on very high resolution PolSAR imagery. Nevertheless, for other applications, say, small object analysis and geophysical parameter estimation, it still plays a significant role. This is due to the fact that the analysis and estimation results of such applications are often sensitive to speckle noise. Therefore a quantitative measurement for various filters will make sense in such a context.

4.1 *Indicators for Polarimetric Information*

Diverse parameters have been suggested for characterizing polarimetric information by different researchers. Only the three most related polarimetric parameters will be explored in this study due to limited space.[1]

1. Radiometric parameters. They correspond to three diagonal elements of the covariance matrix. These parameters, denoted by σ, contain the power component of the scattering procedure.
2. Complex correlation parameters. These parameters, representing complex correlation between polarimetric channels, refer to the remaining three off-diagonal terms of the covariance matrix. It is obvious that these terms are composed of amplitude and phase information.
3. Incoherent decomposition parameters. The famous Cloude and Pottier decomposition is derived from the eigen decomposition of the coherency matrix. This set of parameters consists of three items: averaged alpha angle, polarimetric entropy, and anisotropy. The averaged alpha angle, denoted by $\bar{\alpha}$, represents underlying physical scattering mechanisms. The polarimetric entropy, denoted by H, characterizes the degree of statistical disorder of each distinct scattering class. The anisotropy, denoted by A, measures the relative importance of the second and the third eigenvalues of the eigen decomposition. It was pointed out in Ref. [1] that the polarimetric entropy and anisotropy presented some limitations when highlighting the deficiencies of certain filters, because they were defined in a relative way. Under such circumstances it would also be necessary to consider the eigenvalues of the Cloude and Pottier decomposition.

How to evaluate the filtering results in terms of the three categories of parameters seems to be a quandary since it is impossible to judge whether one filter is efficient or not based solely on their numerical magnitude. The absolute relative bias was introduced for assessing the filtering performance in regard to these three categories of parameters.[1] Hence, it is necessary here to put forward at first the formalizing of bias evaluation. Let m denote a PolSAR image and F denote a certain filter. Then the Yamaguchi four-component decomposition will be applied to the experimental sample image.[20] Each pixel is labeled as a certain scattering class, which is denoted by l. For any one of the aforesaid parameters, which is denoted by θ, its corresponding estimate value $\hat{\theta}$ is obtained by calculating the mean value of the pixels in each scattering class. The absolute relative bias of a certain parameter θ is defined as Eq. (5):

$$\Gamma_{\theta,l,m,F} = \left| \frac{\theta_l - \hat{\theta}_l}{\theta_l} \right|. \tag{5}$$

What is noteworthy is that the absolute relative bias will be an infinite number if one parameter is close or equal to zero. As such, a maximum value of 1 is assigned for the calculating result. Additionally, a median operator across all the various scattering classes will be utilized with the purpose of getting an average value. Then the aggregated performance indicators will be acquired using

$$\Gamma_{\theta,m,F} = \underset{l \in \text{all classes}}{\text{median}} \left[\min \left(\left| \frac{\theta_l - \hat{\theta}_l}{\theta_l} \right|, 1 \right) \right]. \tag{6}$$

It was shown clearly that the median operator could, to some extent, eliminate the sensitivity to the presence of outliers and mitigate the dependence of the filtering performances on the type of scattering phenomenon.[1]

4.2 Indicators for Spatial Information

The spatial details have attracted attention in the community of optical image processing and SAR image processing. In general, three indicators, including edge preservation (EP), point target preservation (TP), and equivalent number of looks (ENL), are employed to evaluate the filtering performance with regard to the preservation of spatial information.

(1) EP. This quantitative index is defined as the average ratio between the observed gradient values on the diagonal elements of the filtered image and the gradient values on the ground truth image. Such an index makes little sense because the imagery itself contains indeterminate noise. As for the real PolSAR imagery, the ground truth image for a real scenario is often absent. As such this item is excluded in the following experiment.

(2) TP. Point targets usually correspond to some important objects, such as artificial buildings and metal objects, in a scene. Detecting this kind of target is indispensable to interpretation and other applications in PolSAR image processing. As is known to all, point TP should be evaluated on the span image as Eq. (7). The half power point width, i.e., -3 dB point, along the horizontal and vertical axes is calculated for quantitatively characterizing the amount of smoothing after speckle filtering. The ratio of half power point width, denoted by operator Δ, between the original span image and filtered span image is suggested to be a quantitative indicator when evaluating the point TP:

$$\text{TP} = \sum_{(x,y) \in \text{point target}} \left(\frac{\Delta_{x,-3 \text{ dB}} S \Delta_{y,-3 \text{ dB}} S}{\Delta_{x,-3 \text{ dB}} \hat{S} \Delta_{y,-3 \text{ dB}} \hat{S}} \right). \tag{7}$$

(3) ENL. First, the standard deviation to mean ratio is defined for the pixels in a homogeneous area, which is denoted as Eq. (8). Second, the ENL for intensity image is defined as Eq. (9). It can be seen formally that the higher the ENL is, the lower the speckle level is. Regardless of doubt from a small number of researchers, this index has been widely accepted in the community.

$$\beta = \frac{\text{standard deviation}}{\text{mean}}, \tag{8}$$

$$\text{ENL}(I) = \frac{1}{\beta^2}. \tag{9}$$

4.3 Real Polarimetric Synthetic Aperture Radar Data for Evaluation

The real PolSAR data to be evaluated is obtained from the UAVSAR system. UAVSAR is an L-band imaging radar instrument that uses microwaves in the 1.2 GHz range to detect and measure objects.[21] The sample data used in the evaluation were acquired on April 2, 2015, over the area of Rosario, which is the largest city in the province of Santa Fe, in central Argentina. This original sample data have 93,119 pixels in the azimuth direction and 9900 pixels in the range direction. The corresponding slant postpixel spacing is 0.6 m in the azimuth direction and 1.66 m in the range direction. The sample data have been multilook processed with 7759 pixels in the azimuth direction and 3300 pixels in the range direction. Then the slant postpixel spacing becomes 7.2 m in the azimuth direction and 4.99 m in the range direction. For the sake of low computational complexity, a subregion with 3900 pixels in the azimuth direction and 1700 pixels in the range direction is cropped as an experimental object.

4.4 *Results and Discussion*

Eight filters, namely, boxcar, SMB,[6] LeeSig,[7] MB,[8] An-Yang,[12] NM,[13] MS,[14] and Sun[15] mentioned in Sec. 3, will be quantitatively evaluated in this section. The abbreviation "original" means the downloaded multilook complex data without any processing. The window size is set to be 5×5 pixels when applying the Cloude–Pottier decomposition. The numbers in parenthesis refer to the value of the diffusion step and total diffusion time. The Pauli image of the sample data set is presented in Fig. 1. As regards the evaluation of those indicators of polarimetric information, the procedure must be done within stationary regions away from the boundary pixels. Nevertheless, it is scarcely possible to manually or automatically select an absolutely stationary region due to the complexity of the natural scenario. Therefore, a relatively stationary region as a substitute will be selected manually to achieve this aim. Two quadrilateral subareas are singled out and marked with red lines as a representative sample of stationary regions. The area with number 1 is a large parking lot that is surrounded by vegetation. Another area with number 2 is a small forest located at the west bank of the Parana river. The parameters for these areas are presented in Table 1. Detailed quantitative measuring results of indicators for polarimetric information are listed in Tables 2 and 3. On the whole, minor differences can be seen

Fig. 1 The Pauli image of sample data over the area of Rosario, Argentina. This image has been applied a multilook of three looks in range and 12 looks in azimuth. (UAVSAR data courtesy NASA/JPL-Caltech).

Table 1 Location parameters for two sample areas.

	Area no.1 (parking lot)	Area no.2 (forest)
Top point coordinates	(850, 767)	(1021, 1789)
Left point coordinates	(858, 780)	(1012, 1847)
Right point coordinates	(897, 791)	(1150, 1823)
Bottom point coordinates	(906, 803)	(1143, 1878)

**Table 2** The absolute relative bias of eight filters with regard to indicators for polarimetric information in subarea No. 1.

|	$C11$	H	A	$\bar{\alpha}$
Original	0.5357	0.0737	0.1499	0.0929
Boxcar	0.2254	0.0616	0.1496	0.1187
SMB	0.3558	0.0699	0.1560	0.0975
LeeSig	0.3147	0.0697	0.1294	0.0865
MB	0.1389	0.0415	0.1205	0.0910
An-Yang	0.1108	0.0121	0.1728	0.1761
NM	0.2047	0.0467	0.1394	0.0954
MS	0.1618	0.0225	0.0934	0.0601
Sun (0.01,60)	0.2990	0.0563	0.1458	0.0776
Sun (0.01,100)	0.2931	0.0552	0.1494	0.0760
Sun (0.01,200)	0.2818	0.0533	0.1493	0.0750
Sun (0.05,100)	0.2415	0.0452	0.1481	0.0687

Table 3 The absolute relative bias of eight filters with regard to indicators for polarimetric information in subarea No. 2.

	$C11$	H	A	$\bar{\alpha}$
Original	0.3716	0.0602	0.0727	0.0908
Boxcar	0.1748	0.0573	0.0604	0.0821
SMB	0.1514	0.0490	0.0543	0.0750
LeeSig	0.1528	0.0549	0.0427	0.0832
MB	0.1202	0.0323	0.0484	0.0656
An-Yang	0.1491	0.0410	0.0358	0.0632
NM	0.1692	0.0598	0.0394	0.0857
MS	0.1528	0.0417	0.0373	0.0686
Sun (0.01,60)	0.2299	0.0476	0.0748	0.0749
Sun (0.01,100)	0.2235	0.0471	0.0754	0.0747
Sun (0.01,200)	0.2219	0.0469	0.0764	0.0744
Sun (0.05,100)	0.1919	0.0462	0.0753	0.0723

among these filters for the two experimental areas. For a specific polarimetric parameter, different filters demonstrate distinct performances with respect to absolute relative bias. With reference to radiometric parameter $C11$, filters such as MB, An-Yang, and MS perform slightly better than the others. The MS filter achieves a relatively optimal performance in respect of three Cloude–Pottier parameters for the two experimental areas. The bias indicator of original data is almost larger than that of any of the eight filters with reference to the three Cloude–Pottier parameters. This phenomenon may be attributed to a slightly larger window size when applying the Cloude–Pottier decomposition. It is surely a dilemma that too large an
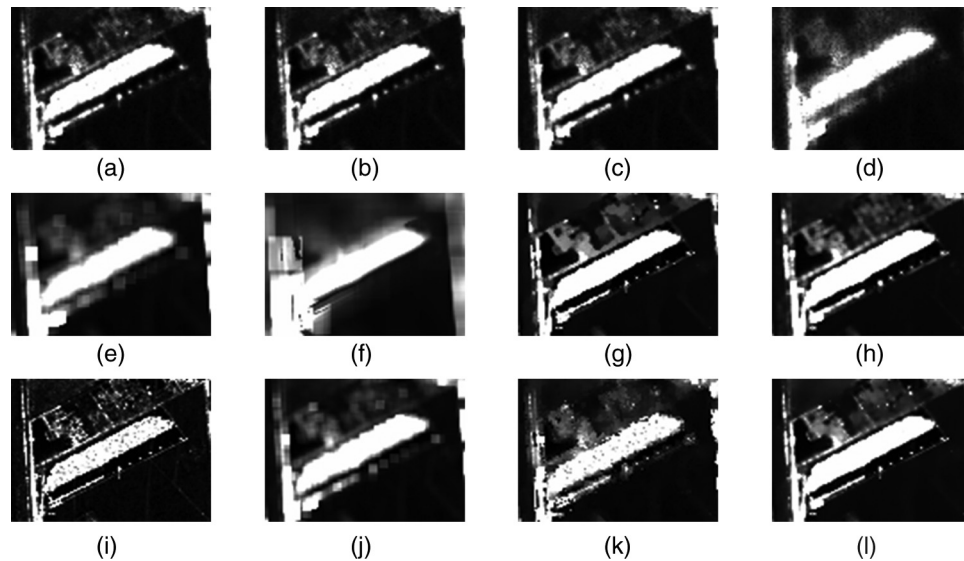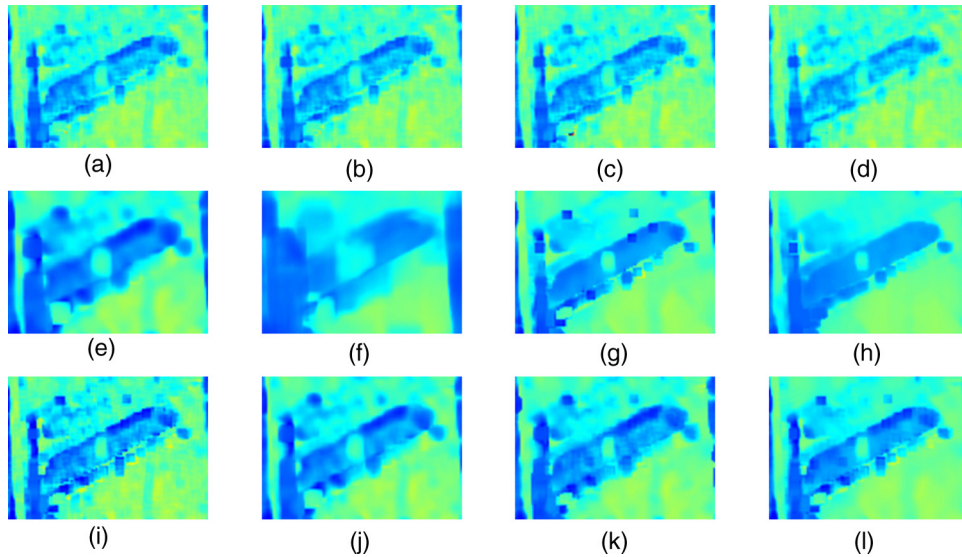

Fig. 2 The intensity image of area no. 1 for the channel $C11$. (a) The original subarea before filtering. (b–h) The results being filtered by boxcar, SMB,[6] LeeSig,[7] MB,[8] An-Yang,[12] NM,[13] and MS[14] filter, respectively. (i–l) The results of Sun[15] filter being diffused by 60 iterations with step size 0.01, 100 iterations with step size 0.01, 200 iterations with step size 0.01, and 100 iterations with step size 0.05, respectively.
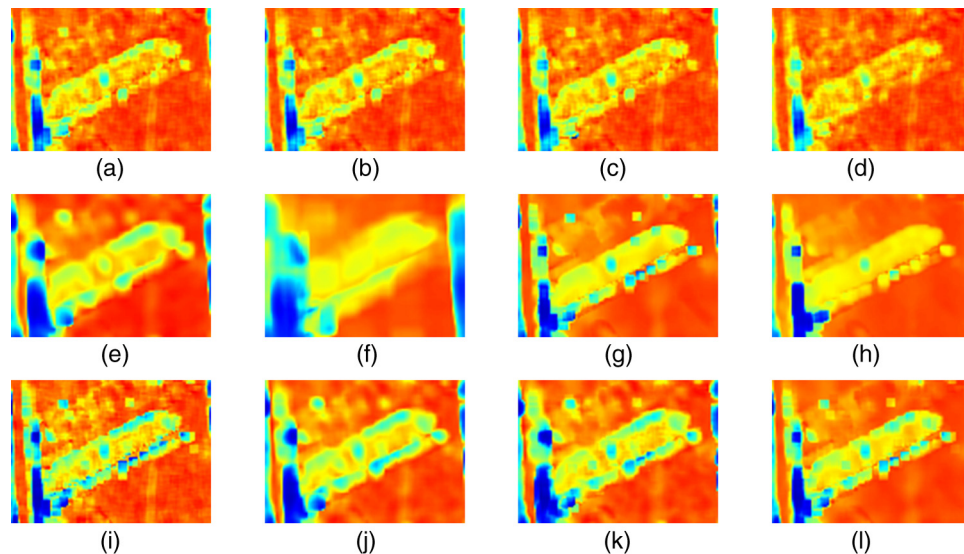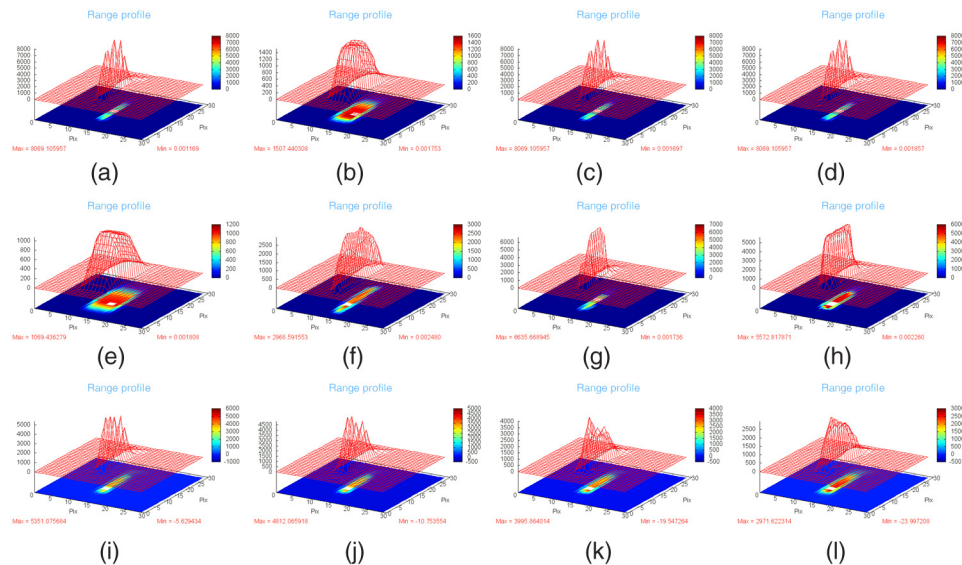

Fig. 3 The pseudocolor image of area no. 1 for the entropy parameter. (a) The original subarea before filtering. (b–h) The results being filtered by boxcar, SMB,[6] LeeSig,[7] MB,[8] An-Yang,[12] NM,[13] and MS[14] filter, respectively. (i–l) The results of Sun[15] filter being diffused by 60 iterations with step size 0.01, 100 iterations with step size 0.01, 200 iterations with step size 0.01, and 100 iterations with step size 0.05, respectively.

averaging window may be more likely to introduce heterogeneous pixels and too small an averaging window may cause an inadequate number of looks. It can also be seen that the Sun filter is convergent with the increase of diffusion times. Therefore, the smaller bias can be achieved by adding the iterative filtering times.

The visual results of area no. 1 for the parameter $C11$ are presented in Fig. 2. Similarly, the visual results for the entropy and averaged alpha angle parameters are presented in Figs. 3 and 4, respectively. Two vessel targets were sailing up the Parana river in the scene. Since the hull of the vessel is composed of metal, they can be viewed as point targets. The data profiles of the area

Fig. 4 The pseudocolor image of area no. 1 for the averaged alpha angle parameter. (a) The original subarea before filtering. (b–h) the results being filtered by boxcar, SMB,[6] LeeSig,[7] MB,[8] An-Yang,[12] NM,[13] and MS[14] filter, respectively. (i–l) the results of Sun[15] filter being diffused by 60 iterations with step size 0.01, 100 iterations with step size 0.01, 200 iterations with step size 0.01, and 100 iterations with step size 0.05, respectively.

Fig. 5 The three-dimensional (3-D) mesh plots of point target for $C11$ parameter. (a) The original 3-D mesh plot before filtering. (b–h) The results being filtered by boxcar, SMB,[6] LeeSig,[7] MB,[8] An-Yang,[12] NM,[13] and MS[14] filter, respectively. (i–l) are the results of Sun[15] filter being diffused by 60 iterations with step size 0.01, 100 iterations with step size 0.01, 200 iterations with step size 0.01, and 100 iterations with step size 0.05, respectively.

where the vessel target is located are presented in Fig. 5 with the purpose of displaying the alteration of point targets after speckle filtering.

Quantitative measuring results of indicators for spatial information are listed in Tables 4 and 5. What is noteworthy is that conspicuous performance differences of these filters can be seen in the two tables in respect to ENL and TP. The An-Yang filter has a relatively poor performance concerning the point TP, although it achieves a remarkable performance with respect to ENL. Just as with the An-Yang filter, MB, NM, and MS do not perform well concerning the point TP, while they do very well with regard to ENL. An outlier with the value 1.1744 can be noticed for the NM filter. This phenomenon results from the alteration of the center pixel of point targets.

Table 4 The filtering results of eight filters with regard to indicators for spatial information in subarea No. 1.

	ENL	TP
Original	0.9739	
Boxcar	5.0839	0.1842
SMB	1.0882	1.0000
LeeSig	1.3547	1.0000
MB	7.7178	0.1271
An-Yang	53.4173	0.3254
NM	2.7435	1.1744
MS	3.4991	0.2903
Sun (0.01,60)	2.1727	0.7103
Sun (0.01,100)	2.2930	0.7097
Sun (0.01,200)	2.4714	0.5302
Sun (0.05,100)	4.9013	0.3508

Table 5 The filtering results of eight filters with regard to indicators for spatial information in subarea No. 2.

	ENL	TP
Original	2.3739	
Boxcar	8.1968	0.0547
SMB	7.4625	1.0000
LeeSig	12.7775	1.0000
MB	10.5017	0.0342
An-Yang	36.1085	0.0774
NM	10.3521	0.6672
MS	28.8906	0.4562
Sun (0.01,60)	5.4024	0.6581
Sun (0.01,100)	5.6438	0.4958
Sun (0.01,200)	5.8797	0.1805
Sun (0.05,100)	9.1801	0.1232

The LeeSig and SMB filters perform very well with regard to the point targets preservation, while they have medium performances with regard to ENL. The reason why the two filters preserve point targets successfully is that they distinguish point targets according to the 98% of the power of the selected channel. However, this schema adopting a hard threshold value is not a one-size-fits-all-approach. The Sun filter demonstrates medium performances both in ENL and TP. The more the diffusion times, the higher the ENL is and the lower the TP is.

5 Conclusions

A comparative evaluation of existing speckle filters has been presented, in the context of a very high-resolution PolSAR dataset. As a result, there exists a certain degree of performance difference among the various filters in terms of polarimetric information and spatial information indicators. It is noticeable that none of selected filters can simultaneously preserve both the polarimetric information and spatial information flawlessly. The choice of filters depends almost completely on the later applications. In other words, it is essential to take into account the parameter to be exploited when choosing the filter from the candidate list. This evaluation work aims to propose some heuristic guidelines when designing a new speckle filter. The first aspect consists of involving only the stationary set of pixels when exploring spatial or polarimetric information. The second and last aspect consists of adaptation to polarimetric information and spatial information that should be jointly considered. In short, speckle filtering remains a theme that deserves further attention with the emergence of very high-resolution spaceborne and airborne PolSAR missions.

Acknowledgments

References

1. S. Foucher and C. Lopez-Martinez, "Analysis, evaluation, and comparison of polarimetric sar speckle filtering techniques," *IEEE Trans. Image Process.* **23**(4), 1751–1764 (2014).
2. O. D'Hondt, S. Guillaso, and O. Hellwich, "Iterative bilateral filtering of polarimetric SAR data," *IEEE J. Sel. Top. Appl. Earth Obs. Remote Sens.* **6**(3), 1628–1639 (2013).
3. P. A. Rosen et al., "Uavsar: new NASA airborne SAR system for research," *IEEE Aerosp. Electron. Syst. Mag.* **22**(11), 21–28 (2007).
4. T. Fujimura et al., "A new small airborne SAR based on pi-SAR2," in *IEEE Int. Geoscience and Remote Sensing Symp.*, pp. 4483–4486 (2013).
5. J.-S. Lee, T. L. Ainsworth, and Y. Wang, "On polarimetric sar speckle filtering," in *IEEE Int. Geoscience and Remote Sensing Symp.*, pp. 111–114 (2012).
6. J.-S. Lee et al., "Scattering-model-based speckle filtering of polarimetric SAR data," *IEEE Trans. Geosci. Remote Sens.* **44**(1), 176–187 (2006).
7. J.-S. Lee et al., "Improved sigma filter for speckle filtering of SAR imagery," *IEEE Trans. Geosci. Remote Sens.* **47**(1), 312–324 (2009).
8. C. López-Martínez and X. Fabregas, "Polarimetric SAR speckle noise model," *IEEE Trans. Geosci. Remote Sens.* **41**(10), 2232–2242 (2003).
9. S. Foucher and C. López-Martínez, "An evaluation of polsar speckle filters," in *IEEE Int. Geoscience and Remote Sensing Symp.*, pp. 845–848 (2009).
10. C. Lopez-Martinez and X. Fabregas, "Model-based polarimetric SAR speckle filter," *IEEE Trans. Geosci. Remote Sens.* **46**(11), 3894–3907 (2008).

11. C. López-Martínez and A. Alonso-González, "Past and new trends in polarimetric and multidimensional SAR data speckle noise filtering," in *IEEE Int. Geoscience and Remote Sensing Symp.*, pp. 45–48 (2014).

12. J. Chen et al., "Nonlocal filtering for polarimetric SAR data: a pretest approach," *IEEE Trans. Geosci. Remote Sens.* **49**(5), 1744–1754 (2011).

13. H. Zhong, J. Zhang, and G. Liu, "Robust polarimetric SAR despeckling based on nonlocal means and distributed lee filter," *IEEE Trans. Geosci. Remote Sens.* **52**(7), 4198–4210 (2014).

14. F. Lang et al., "Mean-shift-based speckle filtering of polarimetric SAR data," *IEEE Trans. Geosci. Remote Sens.* **52**(7), 4440–4454 (2014).

15. S. Sun et al., "Anisotropic diffusion for speckle filtering of polarimetric synthetic aperture radar imagery," *J. Electron. Imaging* **22**(1), 013003 (2013).

16. J.-S. Lee and E. Pottier, *Polarimetric Radar Imaging: From Basics to Applications*, CRC Press, Boca Raton (2009).

17. A. Marino, S. R. Cloude, and I. H. Woodhouse, "A polarimetric target detector using the Huynen fork," *IEEE Trans. Geosci. Remote Sens.* **48**(5), 2357–2366 (2010).

18. A. Marino, S. R. Cloude, and J. M. Lopez-Sanchez, "A new polarimetric change detector in radar imagery," *IEEE Trans. Geosci. Remote Sens.* **51**(5), 2986–3000 (2013).

19. J.-S. Lee et al., "Polarimetric SAR speckle filtering and the extended sigma filter," *IEEE Trans. Geosci. Remote Sens.* **53**(3), 1150–1160 (2015).

20. Y. Yamaguchi et al., "Comparison of model-based four-component scattering power decompositions," in *Asia-Pacific Conf. on Synthetic Aperture Radar*, pp. 92–95 (2013).

21. A. G. Fore et al., "Uavsar polarimetric calibration," *IEEE Trans. Geosci. Remote Sens.* **53**(6), 3481–3491 (2015).

Sheng Sun received his MS and PhD degrees from Huazhong University of Science and Technology, Wuhan, China, in 2006 and 2013, respectively. He is now with the School of Computer Science, Guangdong University of Technology. His research interests include polarimetric synthetic aperture radar imagery processing, remote sensing, and computer vision.

Renfeng Liu received his PhD in pattern recognition and intelligent system from Huazhong University of Science and Technology in 2012. Now he is an assistant professor at the School of Information Engineering, Guangdong University of Technology, China. His research interests include pattern recognition and computer vision.

Changcai Yang received his PhD in pattern recognition and intelligent systems from the School of Automation, Huazhong University of Science and Technology in 2012. He worked as postdoctor at the Huazhong University of Science and Technology from 2012 to 2014. He is now a lecturer at the College of Computer and Information Science, Fujian Agriculture and Forestry University, Fuzhou, China.

Huabing Zhou received his PhD in pattern recognition and intelligent systems from the School of Automation, Huazhong University of Science and Technology in 2012. He is now with the Hubei Provincial Key Laboratory of Intelligent Robot, Wuhan Institute of Technology, Wuhan, China.

Ji Zhao received his PhD in pattern recognition and intelligent systems from the Huazhong University of Science and Technology in 2012. From 2012 to 2014, he was a research associate at the Robotics Institute, Carnegie Mellon University, Pittsburgh, Pennsylvania, USA. He is now with the SAIT China Lab, Samsung Research Center. His main research topics lie in computer vision and machine learning.

Jiayi Ma is currently an associate professor with the Electronic Information School, Wuhan University, Wuhan, China. He received his PhD in Control Science and Engineering from the Huazhong University of Science and Technology in 2014. From September 2012 to September 2013, he was an exchange student at the Department of Statistics, University of California, Los Angeles, USA, supervised by Prof. Alan L. Yuille. His current research is focused on image matching.